Electronic Supplementary Material (ESI) for Materials Horizons.

Electronic Supplementary Information

Chaotic printing: Using chaos to fabricate densely packed micro- and nanostructure at high resolution and speed

Grissel Trujillo-de Santiago, Mario Moisés Alvarez*, Mohamadmahdi Samandari, Gyan Prakash, Gouri Chandrabhatla, Pamela Inés Rellstab-Sánchez , Batzaya Byambaa, Parisa Pour Shahid Saeed Abadi, Serena Mandla, Reginald Avery, Alejandro Vallejo-Arroyo, Amir Nasajpour, Nasim Annabi, Yu Shrike Zhang, Ali Khademhosseini*

Methodology

*Experimental set-up***.** We built a miniJB system composed of a cylindrical reservoir 1.5 cm in diameter made of poly(methyl methacrylate) (PMMA) (referred to as the external cylinder) and an eccentrically located cylindrical shaft 0.5 cm in diameter (referred to as the internal cylinder). The degree of eccentricity ($E= e/\mathrm{r}$) was set at E=0.34, where e is the distance between the shaft center line and the system center line and r is the diameter of the external cylinder. The rotations of the internal and external cylinder were independently controlled using two mini stepper motors (Nema 11, 3.8V, 0.67 A, Model 11HS12-0674S) controlled by an electronic system consisting of an Arduino UNO module (Arduino, Italy), an electronic card for each motor (EasyDriver; stepper motor driver, SX09402, Sparkfun Electronics, USA), and a 12 V power adapter-converter (US Plug AC 100-240V to DC 12 V 2A) (Fig.1). Experiments conducted using PDMS were performed at rotational speeds of 3 RPM (18º s^{-1}) for both the inner cylinder and the outer reservoir. Experiments using GelMA were performed at rotational speeds of 5 RPM (30º s^{-1}) for both the inner cylinder and the outer reservoir. We used different geometrical configurations and mixing protocols to produce regular, partially chaotic, or globally chaotic structures (Fig.S1-S2; ESI). A concentric configuration was used to produce fully regular flows, in which stretching is linear. The cylinders were eccentrically located for the fabrication of partially chaotic or globally chaotic structures. In all cases, the mixing protocol consisted of alternating rotations, in opposite directions, of the external and internal cylinders. The angle of rotation of the external cylinder (αº), and the angle of rotation of the internal cylinder (βº), fully define a mixing protocol: [αº, βº]. The mixing protocol is repeated a number of flow cycles (n); a flow cycle is a complete implementation of one rotation of the external and one rotation of the external cylinder.

Varying the mixing protocol in eccentric configurations then permits the selection of partially or practically globally chaotic flow, in which flow filaments stretch exponentially along the intrinsic flow template or manifold (Fig.S1-S2, ESI). Two chaotic JB recipes were primarily used in this work: (a) [270º, 810°]; and (b) [720º, 2160°]. Mixing protocols were applied for a number of flow cycles (n), ranging from n=3 to n=7.

*Printing experiments***:** Our printing experiments consisted of dispersing small volumes of a viscous suspension or solution (an ink) into a viscous fluid (matrix). For most experiments, the ink injection was located below the liquid surface of the JB reservoir, approximately at the center line of the system and at the mid-point of the gap between the internal cylinder and the internal wall of the external cylinder. We conducted sets of experiments using different cross-linkable or curable materials and diverse "inks" to illustrate the characteristics of the constructs produced by the application of this technique, to confirm its robustness and flexibility and to demonstrate its potential in various applications. PDMS and GelMA[1] were used as the main matrix fluids for printing experiments. Diverse inks were used to illustrate different applications of 3D chaotic printing: suspensions of fluorescent particles to reveal the microstructural features of chaotic and regular flow recipes; gelatin to fabricate sacrificial convoluted empty spaces within GelMA constructs; HUVEC and 3T3 cell suspensions in GelMA-VEGF to print tissue-like microstructures; MCF7 and MCF10A cells to bioprint constructs where cancerous and healthy breast tissues co-exist; green florescent protein (GFP) and red fluorescent protein (RFP) *Escherichia coli* bacteria to print bacterial consortia sharing different degrees of interface; and biotinylated enzymes (i.e., glucose oxidase and peroxidase; Sigma Aldrich; USA) immobilized to streptavidin-functionalized nanoparticles (MagVigen™; Cat# 21005; USA) to print biocatalytic membranes in GelMA constructs; and gold and carbon nanoparticles (Sigma Aldrich; USA), and silver nanowires (ACS Materials; cat# Agnws-200; USA) to print microstructures using nanoparticles.

The microstructure fabricated by the mixing process was preserved by curing at room temperature for 24 hours for the PDMS construct, or UV light exposure (30 seconds; output power of 850 mW at a distance of ~5 cm, using an OmniCure® S2000 system) for GelMA based structures.

Preparation of polymer: PDMS was prepared by mixing a PDMS pre-polymer solution and curing solution (Dow Corning Sylgard 184 Silicon Encapsulant, clear kit, Dow Corning; USA) in a 9:1 volumetric ratio. GelMA (5%) was prepared by dissolving 150 mg of freeze dried GelMA, prepared as described in literature, in a solution consisting of 15 mg of photoinitiator (Ciba Irgacure® 2959, from BASF, Germany) in PBS. This GelMA suspension was vortexed repeatedly during incubation at 70 °C until dissolution. GelMA-VEGF (GelMA covalently functionalized with VEGF) was prepared according to protocols reported before[2]. Briefly, Vascular Endothelial growth factor was covalently conjugated to GelMA using the *N′*-ethyl-carbodiimide hydrochloride (EDC)/*N*-hydroxysuccinimide (NHS) coupling chemistry. Before coupling, GelMA was reacted with an excess amount of succinic anhydride at 50° C to convert most of the lysine amine groups into carboxylic acid groups and minimize side reactions during EDC coupling. Carboxylic acid groups were then activated by reacting with EDC/NHS at room temperature, and VEGF conjugation was achieved by the formation of amide linkages. Gelatin was prepared by dispersing 5 g of porcine skin gelatin (Sigma-Aldrich, USA) in 95 g of phosphate buffer solution (PBS) (Gibco™ Cat No. 14200-075; Thermo Fisher, USA), incubating 60 minutes at room temperature, and heating the solution in a water bath at 70 °C until dissolution. The gelatin solution was used at room temperature in the chaotic printing experiments.

Microstructure analysis: The microstructural features of the fabricated constructs were analyzed by optical microscopy using a fluorescence optical microscope (Zeiss, USA), or by confocal microscopy. Nanostructure alignment was verified using a scanning electron microscope (SEM) (Quanta 200 FEG, FEI™) under high vacuum or a Merlin High-resolution SEM (Zeiss, USA). Samples were gold or carbon coated with a Gatan High Resolution Ion Beam Coater.

CFD Simulations: We conducted simplified 2D simulations to determine the value of Λ for different JB flows, as well as 3D finite element method (FEM) simulations to characterize the full 3D dynamic behavior of our miniJB system. The Λ value was estimated by idealizing the JB system as a 2-dimensional (2D) flow and a FEM was implemented in COMSOL Multiphysics 4.4 using rotating machinery, laminar flow, and particle tracing for fluid flow physics. Different positions of injection were compared and Λ at different flow locations was estimated by conducting a simulation with 8 line-increments on the centerline passing the centers of two circles. Simulations were performed at a rotational speed of 5 RPM (same rotational speed used in experiments) for both the inner and outer cylinder walls; the fluid kinematic viscosity was set at 1 Pa s and both the solid particles (d=10 μm) and the matrix fluid were considered equal to 1.0 g cm^{-3}. For the purpose of the simulation of the flow field and microstructure of the 3D cases, we solved the Navier-Stokes equations of motion in a 3D grid build in COMSOL Multiphysics 4.4. using rotating machinery, laminar flow, and particle tracing for fluid flow physics. The geometry of the experimental JB system was closely matched. The simulation was discretized with reasonably fine free triangular elements, and mesh sensitivity studies were conducted to ensure consistency of results.

The rotating machinery formulates the Naiver-Stokes equations in two rotating coordinate systems and couples them within a fixed coordinate system. In particle tracing physics, we used Newtonian formulation for the particle movement in the fluid domains as:

$$\frac{d}{dt}(m_p v) = m_p F(u - v) \quad \text{(S1)}$$

where **u** is the fluid velocity, m_p is the particle mass, **v** is the particle velocity, and F is the drag force per unit mass. The boundary conditions for the fluid flow were used as no-slip, which means that the velocity of the wall is equal to the velocity of the contacting flow.

We conducted simulations of different JB chaotic flows by solving the equations of fluid motion using finite element techniques, and we tracked sets of tracer particles within these flows to simulate the process of dispersion of drops of ink. This allowed a highly accurate prediction of the microstructure produced from the application of a particular mixing protocol.

Estimation of the Lyapunov exponent (Λ): Our computer simulations allowed the approximation of Λ for different JB chaotic flows. The Λ value of this globally chaotic flow was calculated by computational simulation of the convection of a string of 100,000 points through five flow cycles (every half-cycle), and then plotting the sum of the distances between consecutive points (the length of the filament) versus time (Fig.3).

In particular, we calculated and recorded, every half-a-cycle, the evolution of the length of a filament initially located at the center line between the two cylinders as they rotated at 5 RPM—this was done both for a globally chaotic miniJB case [270º, 810°] and for a regular flow case [270º, 810°] (centered JB configuration). A *Lyapunov* exponent value (for the chaotic case) was determined from the slope of the linear version of equation 1 (Fig.3).

Additional notes on chaotic printing

In this paper, we have exploited the intrinsic potential of chaotic flows to fabricate fine and aligned structures at an exponential rate to develop predictable microstructures within solidifiable materials in a process that we refer to as chaotic 3D printing. Chaotic printing is inspired in the physics of nature. Complex structures are one of the signatures of nature, and yet the processes that drive the creation of these structures are often simple and iterative [3,4]. The iterative character of natural processes enables the creation of progressively finer patterns, moving from macro to micro and even nano-scales (e.g., fractal processes and geometries). The creation of complex structures is often governed by chaotic processes[5,6].

MiniJB chaotic printer configuration

We have built miniaturized chaotic printers controlled by an Arduino Uno system (Fig.1); these printers are capable of printing high-resolution, highly packed 3D microstructures in small volumes.

Most of the results presented in this work were generated using chaotic recipes operated in a small Journal Bearing (miniJB) flow system. The geometry of the miniJB is inspired by the JB flow originally presented by Swanson and Ottino[7]; however, we introduced relevant modifications that significantly alter its flow dynamics to favor the development of fully 3D chaotic flows. By design, the JB of Swanson and Ottino behaved essentially as a 2D flow system, as the bottom surface of the outer cylinder did not rotate. The authors avoided a zero-velocity boundary condition by adding a layer of high density oil at the bottom of the system. This established a nearly free-flow bottom boundary condition and allowed a close approximation of the dynamic behavior of a 2D chaotic system (with similar boundary conditions at the top and the bottom). By contrast, we purposely rotate the bottom surface (and we avoid the use of a bottom liquid layer). The top–bottom geometric asymmetry in boundary conditions—a free surface at the top and a rotating boundary at the bottom—induces flow asymmetry and enables the establishment of fully 3D chaotic flows. The characteristics of our miniJB flow system are presented in Fig.1a. Fig.1b,c show actual images of a miniJB chaotic printer connected to its Arduino controller.

Notes on chaotic printing using JB flows

The occurrence of chaos in the JB system, or in any potentially chaotic system, depends on geometry factors and operational conditions. In the JB flow, the off-centered location of the inner cylinder is a mandatory requisite for producing chaotic flows (Fig.S1). Concentric JB configurations result in regular flows, where lines, surfaces, or volumes (i.e., filament segments or drop interfaces) will undergo only linear stretching in the direction of the flow lines (Fig.S1a,c). However, in eccentric (off-centered) configurations, the geometric symmetry of the system is broken, resulting in an additional degree of freedom. This simple geometric change enables the generation of chaotic flows under specific operational protocols (Fig.S1b,d).

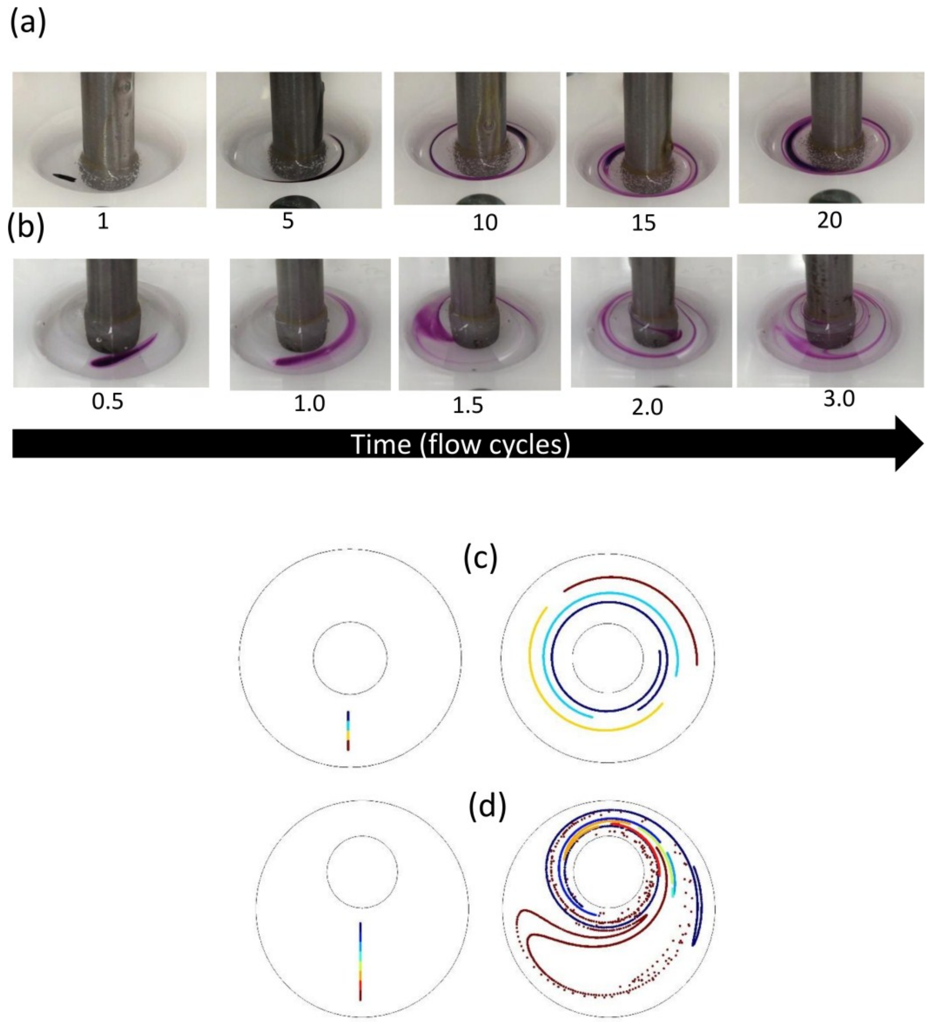

Fig.S1. The miniJB flow can produce either regular or chaotic flows. The geometry of the system (i.e., whether the internal cylinder is located concentrically or off-centered) and the rotation protocol determine the extent of chaos in the miniJB system. While (a) a concentric system will generate only regular motion, (b) an eccentric (off-centered) configuration and a suitable rotation protocol will produce a chaotic flow. (c) Simulated evolution of the microstructure developed from the stretching of different segments (shown in different colors) in a regular flow originated by a concentric system [270°, 810°] at n=3, and (d) in a chaotic flow originated in an eccentric system [270°, 810°] at n=3.

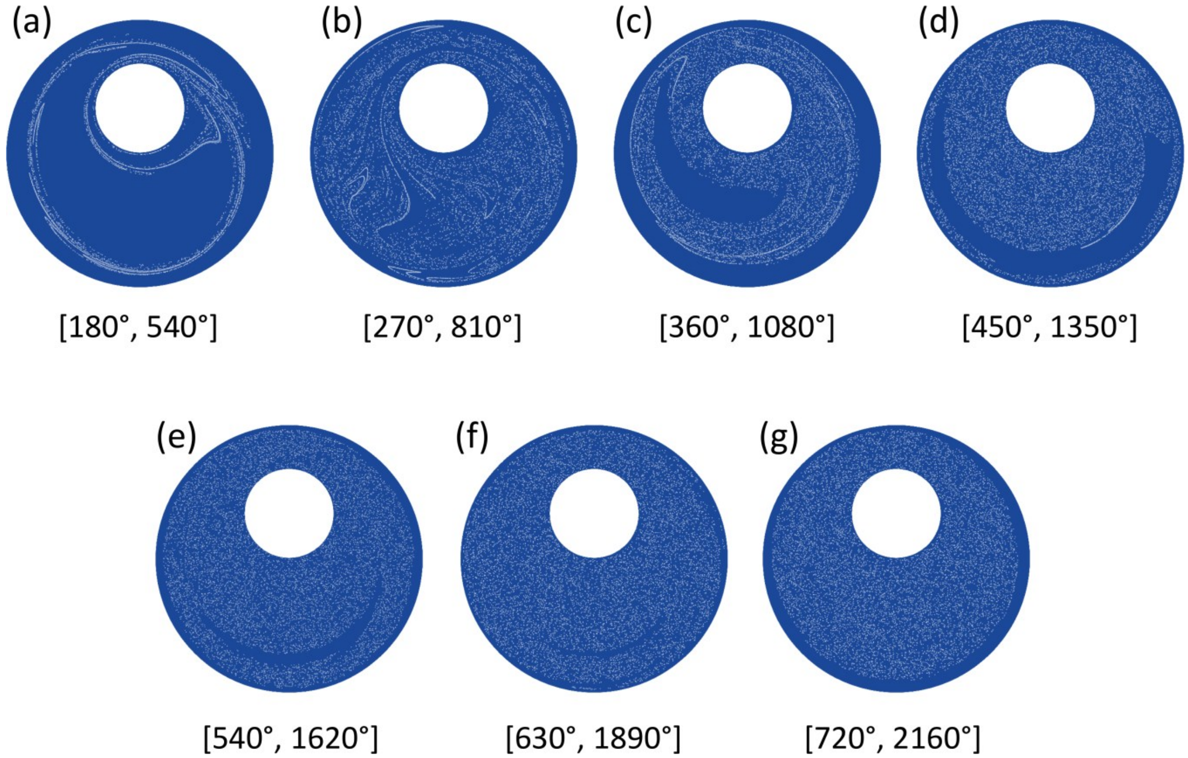

Fig.S2. Different JB mixing protocols generate different microstructures. The microstructure produced by the application of different JB mixing protocols is shown, as calculated by 2D simulations. Selection of certain protocols of rotation results in the generation of either regular, partially chaotic, or globally chaotic flows within the reservoir. (a) A partially chaotic flow with vast islands of regular motion (zones not visited by particles) results from the application of the protocol [180°, 540°]; whereas (b) a practically globally chaotic flow originates by the application of the protocol [270°, 810°]. (c–f) Partially chaotic flows give rise to islands of regular flow of different sizes and in different locations. (g) An essentially globally chaotic flow, with a high *Lyapunov* (Λ) value, is generated by the application of the flow recipe [720°, 2160°]. All microstructures correspond to the dispersion of a circular injection of 10,000 particles, after the application of 10 flow cycles (n=10).

For example, Fig.S2 shows simulation results that demonstrate the structures rendered by the application of different flow protocols. In this work, a chaotic protocol is designated as two angle values within square brackets (i.e., [αº, βº]), where α is the number of degrees that the outer cylinder is rotated and β is the number of degrees that the inner cylinder is rotated.

On the calculation of the *Lyapunov* exponent

Any material drop exposed to a chaotic flow will exponentially stretch—and consequently elongate—along the skeleton of the flow (or invariable manifold). Any chaotic flow has a well-defined, but heterogeneous, stretching field; in any location of a chaotic flow, the stretching intensity can vary by several orders of magnitude. As an illustration, Fig.S1 shows that the simulated evolution of filaments positioned in several different flow locations in regular (Fig.S1c), and chaotic (Fig.S1d) protocols aligns to the same flow manifold but is not identical (i.e., it proceeds at different speeds, particularly during the first flow cycles). However, a common and useful way to characterize the overall (or average) intensity of a chaotic flow, that is how effectively a chaotic flow creates structure, is by determining an average Λ value.

Several strategies can be used to calculate an average *Lyapunov* exponent. One meaningful way is based on following the deformation of a material line (i.e., a filament composed of thousands of points) in the flow. Fig.3 describes the determination of Λ in detail, based on 2D computational simulations. The units of the *Lyapunov* exponent (Λ) can be converted from cycles to seconds simply by considering the speed of rotation of the cylinders [RPM] and the angle of rotation of the mixing protocol. For instance, at 5 RPM (the rotational speed used in our experiments), Λ=1.61 cycle^{-1} = 2.68 s^{-1} for the mixing protocol [270°, 810°]. At 5 RPM, Λ=3.50 cycles^{-1} = 2.18 s^{-1} for the mixing protocol [720°, 2160°].

Assessment of microstructure properties based on the value of the *Lyapunov* exponent

Chaotic printing enables an exponentially fast, facile, and highly precise fabrication of long sheets of material and fibers in short times. This capability is not achievable by any other currently available printing technique, where the printing process is linear. The length and diameter of the stretched filament resulting from different experimental JB flows can be approximated based on the Λ value and some simplifications.

Example 1: stretching of a segment into a fiber

The following exercise assumes that the chaotic flow deforms and stretches a segment of 1m of length into a fiber. Let us consider a model 2D chaotic flow with a $\Lambda = 1.61$ cycle^{-1} ($\Lambda = 2.68$ min^{-1} at 5 RPM), similar to the JB flow depicted in Fig.3. The total length of any vector within the initial spherical drop (i.e., its diameter) will then elongate at a rate defined by the Λ value: $L_n = L_o \exp(\Lambda n)$. Then, the length of a fiber will grow as dictated by the *Lyapunov* exponent.

As we have shown, both experimentally and computationally, the 3D JB chaotic flows will produce shapes that are more convoluted than simple filaments. Nevertheless, this scenario is a first approximation to illustrate the remarkable potential of a chaotic flow to elongate materials, and produce surface area. For example, chaotic printing creates structure much more rapidly than currently available nozzle-based techniques, which have speed limits of between 10 and 50 µm s^{-1} for resolutions between 5–200 µm[8]. At 50 µm s^{-1}, a nozzle-based 3D bioprinter will print a segment 3.13 m long in 17.38 hours, with a modest resolution of 200 µm. A professional 3D printer, working with standard thermoplastics such as ABS or PLA, will perform the same task in 43.47 minutes at a resolution of 200 µm[9]. That same length of filament can be obtained by chaotic printing in 6 minutes (Table S1).

Example 2: Creation of high resolution microstructure

In chaotic printing, the exponential increase in the amount of interface implies that the distance between consecutive lamellae decreases rapidly because the flow occurs in a closed system. Next, we compare the performance of a chaotic printer versus a hypothetical extrusion bioprinter (which is 10 times faster than currently available bioprinting technology) in terms of their ability to create highly packed microstructures in a small area.

First, we consider a linear printing process (such as the one conducted by an extrusion bioprinter) operating in a square area D × D, where D=10 mm (Fig.S3). The process of creation of structure will be also linear, since its speed is constant in time. For example, let us analyze a printing process with a printing speed of 1.2 mm s^{-1} (while noting that profesional printers perform at this speed[9], and the fastest extrusion bioprinter available today prints at 100 μm s^{-1} [8]). After 1 minute, this printer will print a filament 72 mm long, which is 7.2 times the characteristic length D. This speed will be sustained for the rest of the printing operation. Therefore, the total length of the printed filament will be 7.2, 14.4, 21.6, and 28.8 D after 1, 2, 3, and 4 minutes, respectively. The characteristic length scale of the squared system, (i.e., the length of one of the sides of the square) will then be dissected by 7, 14, 21, and 28 lines during the first four minutes of the printing operation. The average striation thickness (the average distance between neighboring printed segments) after 1, 2, 3, and 4 minutes will be D/7=1428, D/14=714, D/21=476, and D/28= 357 μm, respectively (Fig.S3).

Now consider a chaotic 2D model system operating in the same square 1 cm^2 area. Any linear segment will elongate at an exponentially fast rate under the action of the chaotic flow. An exponential elongation in any area or volume preserving flow implies an exponentially fast and organized decrease in length scales. For example, in a flow with Λ = 1.61 $cycle^{-1}$ (Λ = 2.68 min^{-1} at 5 RPM), similar to that exhibited by the JB flow depicted in Fig.3, an initial segment of 2.5 mm will map into a filament of 1, 5, 25, and 125 mm after 1, 2, 3, and 4 successive flow cycles.

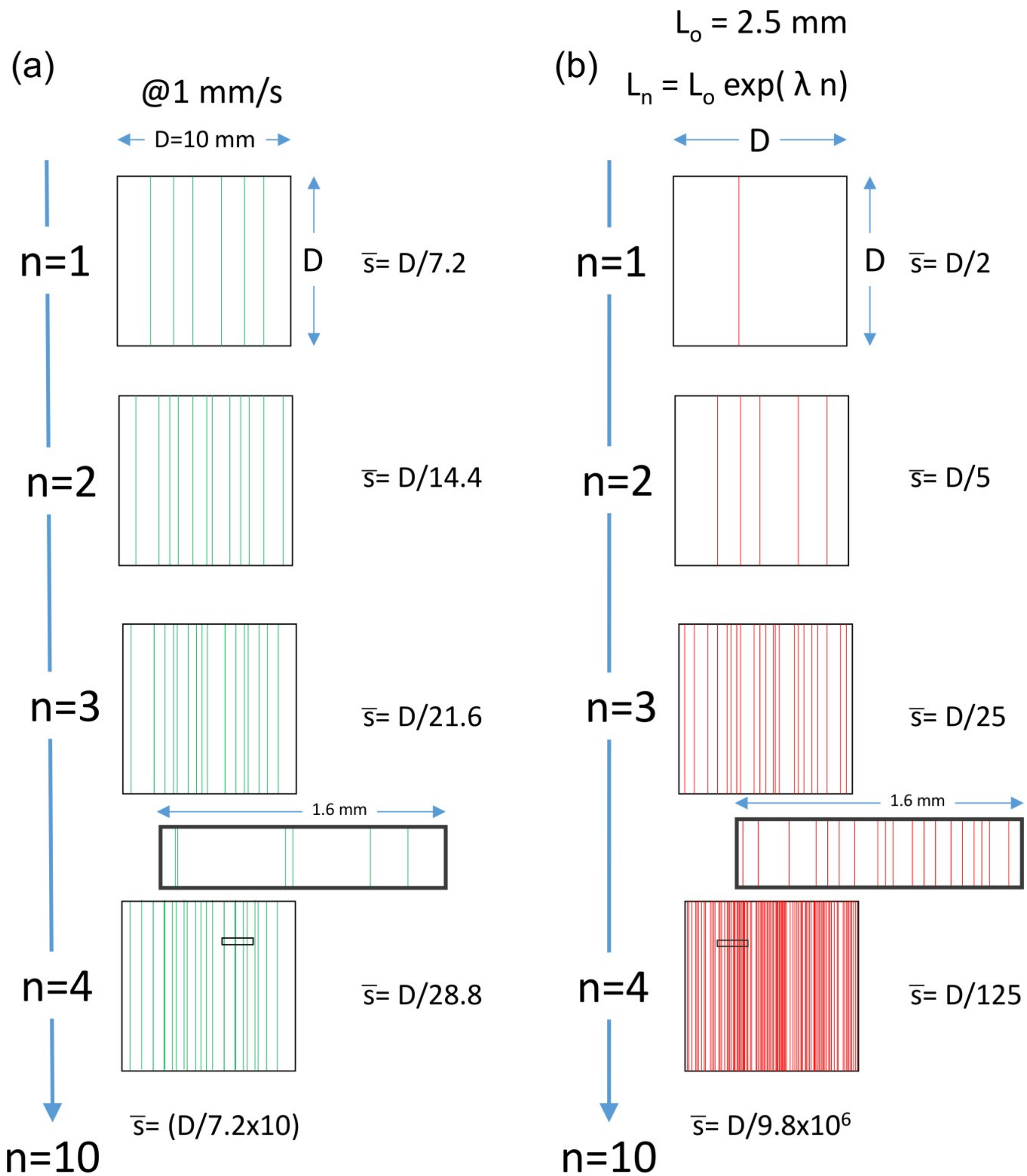

Fig.S3. Exponential reduction of striation thicknesses (distances between printed lines) originated by chaotic printing. (a) A profesional printer reduces the length scales in a squared region at a linear rate. By contrast, (b) a chaotic printer (Λ= 1.61 cycle^{-1}; Λ= 2.68 min^{-1} at 5 RPM) reduces the characteristic length scales (striation thicknesses) at an exponentially fast rate.

The characteristic length scale of the square system (i.e., the length of one of the sides of the square) will then be dissected by 1, 5, 25, and 125 lines for the first four flow cycles, respectively. The average striation thickness after 1, 2, 3, and 4 minutes will be D/1=10000, D/5=2000, D/25=400, and D/125= 80 µm, respectively (Fig.S3; Table S1). Similarly, Table S1 presents a comparisson of the length produced, the number of striations, and the average striation thickness generated by a chaotic printer and an average profesional 3D printer operating at a speed of 1.2 mm/s (~ 10´s of cm^3/h).

Table S1. Comparison of the length of a printed segment (L_n), the number of striations, and the average striation thickness (ṡ) at different times generated by a chaotic printer, and an average 3D printer[9] (printing @ velocity =1.2 mm/s).

	Chaotic printer (Λ=2.68 min^{-1})			Profesional Extrusion 3D printer		
time (min)	**L_n (m)**	**number of striations**	**ṡ (m)**	**L_n (m)**	**number of striations**	**ṡ (m)**
0.0	1.00E-03					
0.6	5.00E-03	5.00E-01	2.00E-02	4.32E-02	4.32E+00	2.31E-03
1.2	2.50E-02	2.50E+00	4.00E-03	8.64E-02	8.64E+00	1.16E-03
1.8	1.25E-01	1.25E+01	7.99E-04	1.30E-01	1.30E+01	7.72E-04
2.4	6.26E-01	6.26E+01	1.60E-04	1.73E-01	1.73E+01	5.79E-04
3.0	3.13E+00	3.13E+02	3.19E-05	2.16E-01	2.16E+01	4.63E-04
3.6	1.57E+01	1.57E+03	6.38E-06	2.59E-01	2.59E+01	3.86E-04
4.2	7.84E+01	7.84E+03	1.27E-06	3.02E-01	3.02E+01	3.31E-04
4.8	3.92E+02	3.92E+04	2.55E-07	3.46E-01	3.46E+01	2.89E-04
5.4	1.96E+03	1.96E+05	5.09E-08	3.89E-01	3.89E+01	2.57E-04
6.0	9.82E+03	9.82E+05	1.02E-08	4.32E-01	4.32E+01	2.31E-04
6.6	4.91E+04	4.91E+06	2.04E-09	4.75E-01	4.75E+01	2.10E-04

As shown in Table S1, the linear printing process is faster during the first two minutes. Ultimately, and soon, the exponential nature of chaotic printing surpasses the ability for microstructure creation of the linear printing process. After 6 minutes, the chaotic printing scheme will generate close to 1 million striations in the squared box (generating an average striation thickness of 10.2 nm). In the same time frame, the linear printing process will have generated only 43 atriations, generating an average striation thickness of 230 µm). Note that currently, the maximum resolution physically achievable by a state of the art 3D printer is 5 µm. This limit is surpased by a chaotic printer after only 4 minutes of printing time.

Chaotic bioprinting of cell-laden constructs

Diverse tissue-like structures can be designed and fabricated simply by varying key parameters in chaotic printing (i.e., choosing between a chaotic, partially chaotic, or regular flow, varying the number of inks, or the seeding cell density). We envision that chaotic printing can be applied to fabricate systems that will enable the study of fundamental questions related to cell–cell interactions at material interfaces with different degrees of vicinity. We chaotically bioprinted different mammalian cell lines in GelMA hydrogel [1] constructs to illustrate some aspects of the technique (Fig.5m,n, and p; Fig.S4). GelMA is a photocrosslinkable material that has been widely used in tissue engineering applications: it contains cell binding domains, it is biodegradable, and it is amenable to microfabrication.

Chaotic flows can be used effectively to provide efficient separation and encapsulation of individual 3T3 fibroblasts along a flow line, thereby enabling single cell studies (Fig.S4a). Varying the initial cell density also allows control of the cell density along the manifold. In a chaotic flow, vectors (or ink particles) located at different locations in the system experience different degrees of stretching. The local values of stretching dictate the distance between particles. In low stretching regions, the cells remain closer, while in high stretching locations, they are more widely spaced. Chaotic printing can be effectively used to create *ad hoc* local microenvironments for cell growth.

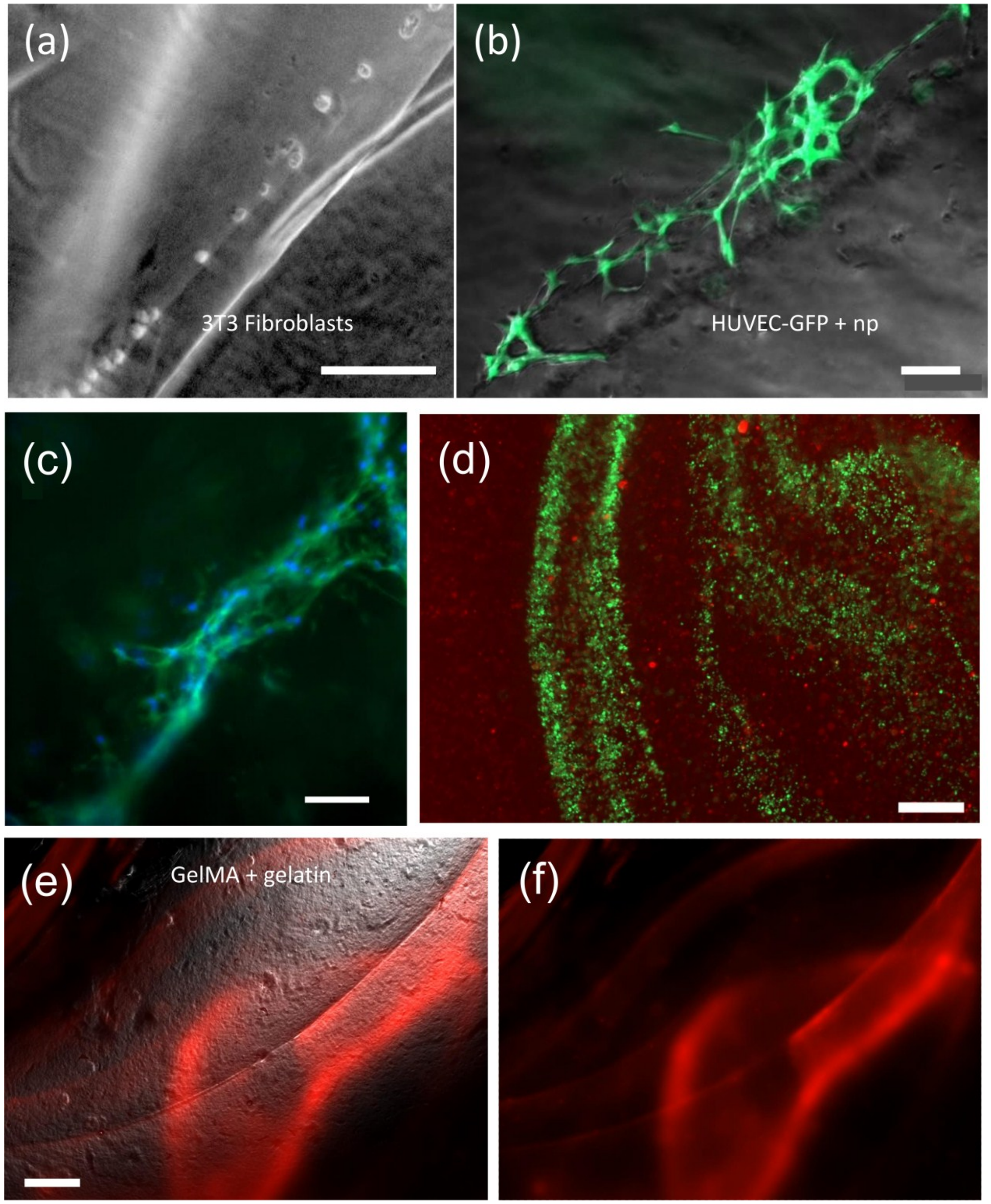

Fig.S4. Chaotic bioprinting of cells for tissue engineering applications. (a) Close-up of a string of NIH3 3T3 fibroblasts aligned by the chaotic flow within a GelMA construct. (b) Segment of a chaotic structure printed using an ink composed of HUVEC-GFP cells and VEGF-conjugated nanoparticles (np). Cells spread along the lines of particles after 5 days of culture. (c) Segment of a chaotic structure printed using an ink composed of HUVEC-GFP cells and VEGF-conjugated nanoparticles, as observed by optical microscopy after 9 days of culture. Cells have been actin-DAPI stained to reveal the position of the nuclei. (d) MCF7 cells (red) and MCF10A cells (green) were co-printed in the same construct. Scale bars: 100 μm. (e) Printing of sacrificial gelatin sheets (rhodamine-stained) within a 3D-GelMA construct, as observed under red fluorescence and bright field illumination, (f) and only red fluorescence (inset). Scale bars: 100 μm.

For example, Fig.S4b shows a string of endothelial cells, growing and spreading in a GelMA construct, after 5 days of culture. These cells were chaotically co-printed with nanoparticles functionalized with VEGF (i.e., the ink was composed of a mix of cells, 5% GelMA, and VEGF attached to nanoparticles) to favor directed and localized cell proliferation and spreading along the manifold lines.

The cell density within the ink to be used and the crosslinking conditions after printing are additional important considerations for chaotic bioprinting. A set of appropriate conditions in terms of these parameters must be determined for each printing experiment. In general, we obtained the best results when we used cell densities of 1×10^7 to 1×10^9 cells mL^{-1} and when we closely matched the viscosity and density of the matrix fluid (i.e. by using the same matrix liquid to suspend cells or particles for ink formulation). Other considerations become important for the bioprinting of specific cell lines. For example, we observed long term survival (up to 15 days), but no cell spreading, in a construct printed using human umbilical vein endothelial cells (HUVECs) in GelMA. Spreading was only observed when the inks contained GelMA and nanoparticles functionalized with VEGF (Fig.S4b,c), or GelMA covalently functionalized with vascular endothelial growth factor [2] (GelMA: 1/10 GelMA-VEGF) (Fig.6a,b,d-e).

In bioprinting experiments, the co-injection of different cell types offers great potential for the fundamental study of cell–cell interactions at different degrees of contact. For example, we have conducted experiments where an ink of breast fibroblast cells in GelMA is bioprinted in a suspension of cancer cells in GelMA (Fig.S4d). In these experiments, MCF7 cells (1.5×10^6 cells mL) were mixed with 5% GelMA and 700 μL this cell suspension was dispensed in the printer reservoir, while 5 μL of an ink composed of 5% GelMA and MCF10A cells (0.8×10^6 cells mL) was initially injected.

Chaotic bioprinting, demands careful control of some operational parameters, mostly related to the matching of the rheology between the matrix liquid and the ink and to the conditions of crosslinking.

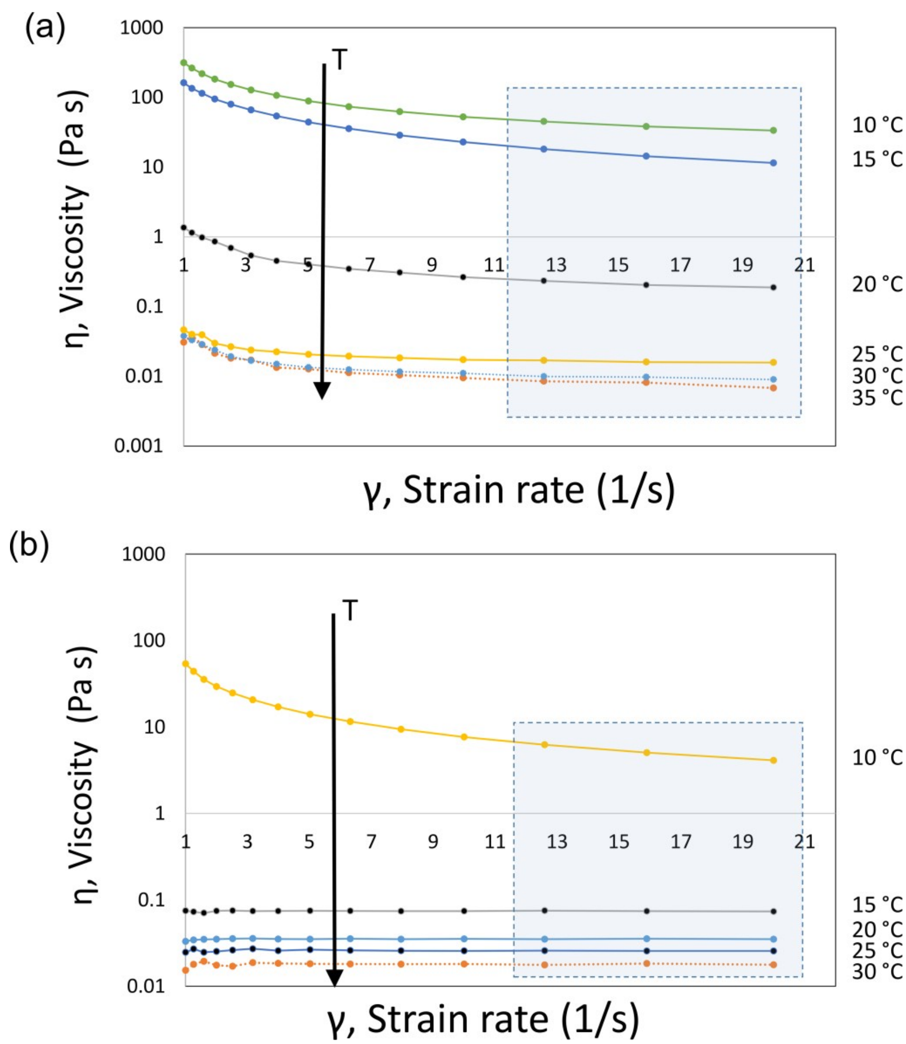

Fig.S5. Rheology window of operation (Newtonian regime) for 3D chaotic printing using GeLMA as a matrix. (a) Viscosity of 10% GelMA pregels at different strain rates (in the low strain regime) and at different temperatures. (b) Viscosity of 5% GelMA pregels at different strain rates (in the low strain regime) and at different temperatures.

Rheology is an important consideration for chaotic printing; the outcome of chaotic printing is predictable for a Newtonian liquid in a laminar regime. GelMA is a complex polymer mixture composed of fragments of collagen molecules of different sizes. However, GelMA pregels (before crosslinking) exhibit a Newtonian behavior in a window of temperatures, concentrations, and strain rates, and possess a conveniently moderate-to-high viscosity that makes them an attractive choice for chaotic bioprinting (Fig.S5).

Alternative experimentally feasible chaotic flows

Most of the results presented here were produced using the miniJB flow system described previously (Materials and Methods and Electronic Supplementary Information). However, chaotic printing can be extended for use with any other experimentally feasible chaotic flow.

For example, Fig.S6 illustrates the use of another experimental system—an experimentally realizable Blinking Vortex—to generate highly packed structures in viscous materials. We have also conducted successful chaotic printing experiments using static mixers, specifically the Kenics mixer. The Kenics mixer is a well-known static mixer that is widely used in the process industries to mix liquids in turbulent and laminar regimes. In laminar flows, the Kenics mixer develops chaotic flows by a mechanism of splitting and stretching.

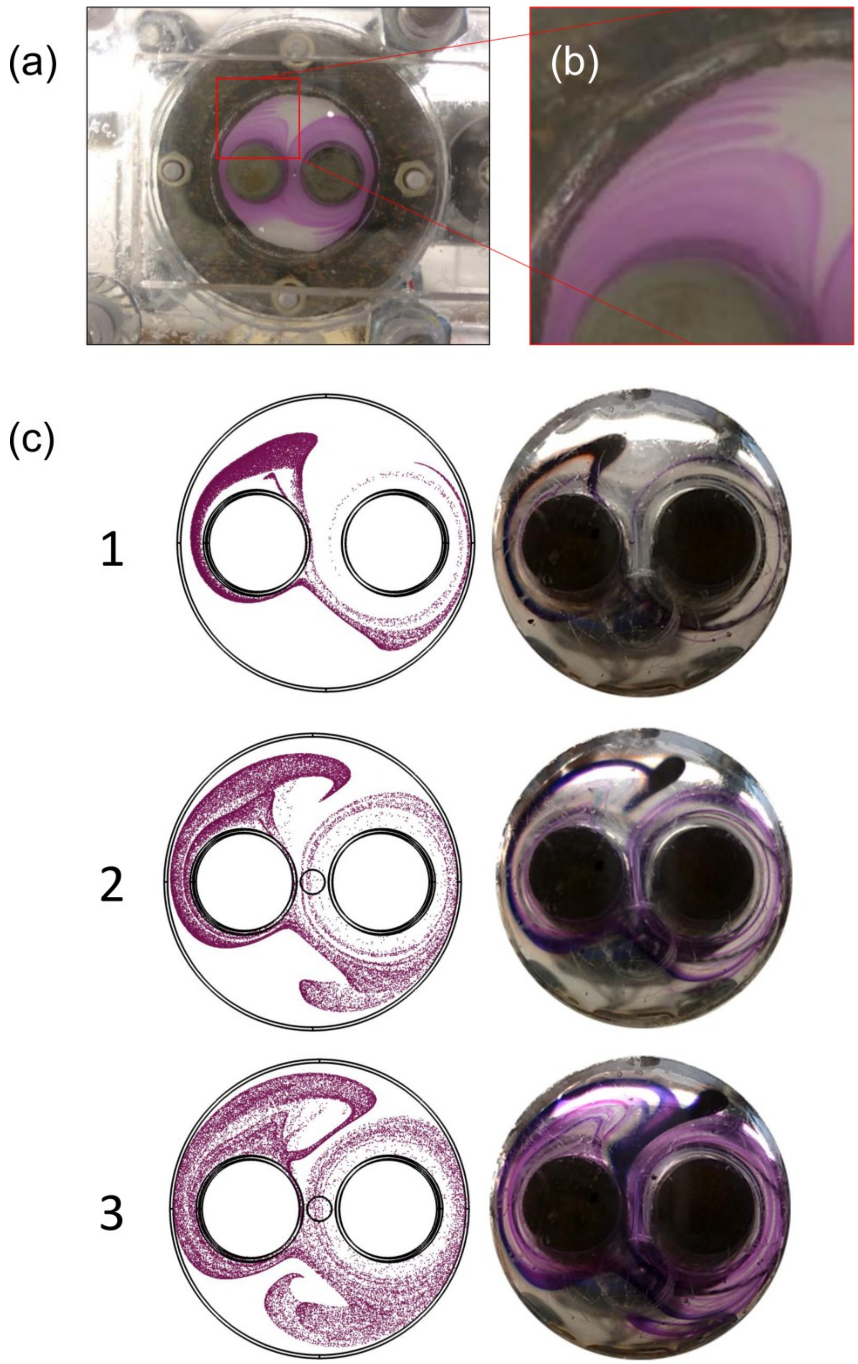

Fig.S6. The blinking vortex (BV): An alternative experimental chaotic flow system. (a) The as-built BV flow system. Two cylinders rotate, in an alternating fashion, in the same direction. In this case, the liquid reservoir (external cylinder) does not rotate and a full flow cycle consists of a 720° rotation of the left internal cylinder and a 2160° rotation of the right internal cylinder [720°, 2160°]. This mixing recipe produces a partially chaotic flow. (b) Close-up of the microstructure experimentally attained with this blinking vortex flow. (c) Comparison of results from 2D simulations and experiments, showing the similarity between the predicted and the experimentally obtained microstructural features after 1, 2, and 3 full flow cycles.

References

1 K. Yue, G. Trujillo-De Santiago, M. Mois Es Alvarez, A. Tamayol, N. Annabi and A. Khademhosseini, *Biomaterials,* **2015**, *73*, 254-71.

2 B. Byambaa, N. Annabi, K. Yue, G. Trujillo-de Santiago, M. M. Alvarez, W. Jia, M. Kazemzadeh-Narbat, S. R. Shin, A. Tamayol and A. Khademhosseini, *Adv. Healthc. Mater.*, 2017, 6,16.

3 T. Tél, A. de Moura, C. Grebogi and G. Károlyi, *Phys. Rep.*, 2005, *413*, 91-196.

4 N. Goldenfeld and L. P. Kadanoff, *Science.* **1999**, 284, 87-89.

5 D. Perugini, G. Poli and R. Mazzuoli, *J. Volcanol. Geotherm. Res.*, 2003, **124**, 255–279.

6 E. E. Zotos, *Chaos, Solitons Fractals Interdiscip. J. Nonlinear Sci. Nonequilibrium Complex Phenom.*, 2011, **44**, 501–509.

7 P. Swanson and J. Ottino, *J. Fluid Mech.*, 1990, **213**, 227–249.

8 S. V Murphy and A. Atala, *Nat. Biotechnol.*, 2014, **32**, 773–85.

9 J. Go, S. N. Schiffres, A. G. Stevens and A. J. Hart, *Addit. Manuf.*, 2017, **16**, 1–11